ACCURACY OF THE MULTIPOLE EXPANSION APPLIED TO A SPHERE IN A CREEPING FLOW PARALLEL TO A WALL

by M. L. EKIEL-JEŻEWSKA[†] *and* E. WAJNRYB

(*Institute of Fundamental Technological Research, Polish Academy of Sciences, Świętokrzyska* 21, 00-049 *Warsaw, Poland*)

[Received 1 April 2006. Revise 25 August 2006]

Summary

An example system is studied to discuss precision of the multipole expansion, applied to determine forces exerted on particles by a viscous low-Reynolds-number fluid flow. A single sphere in an ambient flow (pure shear, quadratic, and modulated shear) parallel to a close plane wall is considered. Forces and torques exerted by the ambient flow on a motionless sphere are evaluated. Their precision is determined and related to a multipole order of the truncation. Similar analysis is performed for a moving sphere with no ambient flow and for a freely moving sphere. Relative motion of the sphere with respect to the wall gives rise to strong lubrication interactions. It is analysed how these interactions affect accuracy of the pure multipole expansion, and what are the smallest distances where it becomes insufficient. An alternative precise method is applied, in which lubrication expressions are subtracted from the hydrodynamic forces and torques, and the residue is evaluated as a fast-convergent series of inverse powers of the distance between the sphere centre and the wall. The accuracy of this procedure is carefully analysed.

1. Introduction

Multipole expansion is widely used to determine transport coefficients and structure of suspensions, and to evaluate hydrodynamic interactions between individual particles in low-Reynolds-number fluid flows; see, for example, (**1** to **3**). This method is adequate to determine the motion of many spherical particles, which undergo external forces in an ambient fluid flow. Periodic boundary conditions, or one or two plane boundaries can be taken into account (**4** to **9**). The multipole method is based on analytical developments, and therefore its precision is controlled. In particular, relative motion of close solid surfaces can be accurately calculated. Such a lubrication correction is implemented in numerical simulations performed also by other methods or for other shapes of the particles; see (**10** to **12**).

The multipole expansion is based on a boundary-integral representation of the velocity and pressure disturbances (**13**, **14**), in conjunction with the use of a Green's tensor for the Stokes equations, suitable for geometry of the system and the boundary conditions. For a fluid bounded by a plane wall, the Green's tensor was given by Blake (**15**). Cichocki and Jones (**16**) used it to combine the multipole expansion with the method of images (**17**). In this approach, the force density and the velocity field at the surfaces of the sphere and of its image are projected on to the complete set

[†]Corresponding author ⟨mekiel@ippt.gov.pl⟩

Q. Jl Mech. Appl. Math, Vol. 59. No. 4
Advance Access publication 23 November 2006. doi:10.1093/qjmam/hbl016

of irreducible multipole functions (**18**). The coefficients of the truncated expansion are determined from the boundary integral equation, which takes the form of a large system of linear algebraic equations. For further details and successful implementations of the irreducible multipole expansion, the reader is directed to the papers by Felderhof, Cichocki, Jones and collaborators, especially to the paper (**19**) for the hydrodynamic interactions between many spheres in infinite space or with periodic boundary conditions. The irreducible multipole expansion was also applied to calculate hydrodynamic interaction of a single sphere with a solid plane wall (**16**) and the results were used to construct theoretical and numerical algorithms for many spheres near a solid plane wall (**7**). Recently, the irreducible multipole expansion has been applied to one sphere between two parallel solid plane walls (**8**, **9**).

Accuracy of the multipole expansion is of great practical interest. Therefore in this paper, an example is studied to discuss the multipole precision: a single sphere, motionless or moving freely, in an ambient flow parallel to a close plane wall. There are three basic goals of this study. First, challenged by the accurate results obtained in the companion paper (**20**) with the use of bipolar coordinates, we have asked what is the 'top precision' of the multipole expansion applied to the same problem, especially for very small distances from the sphere centre to the wall. Secondly, it is of interest to specify how to reach a reasonable relative accuracy, for example, one per cent, using this approach, which could be easily generalized for many spheres. Thirdly, for systems with lubrication between surfaces in relative motion, it is useful to determine the accuracy of the pure multipole expansion (in principle, applicable for relatively large separations of the sphere from the wall) and compare it with the precision of the power-series expansion, performed after subtracting the lubrication expressions (and therefore accurate even for very small separations).

In section 2, we specify the problems; in section 3, we outline how the multipole expansion is applied to solve them. In section 4, we evaluate forces and torques exerted on a motionless sphere by pure shear, quadratic and modulated shear ambient flows. We estimate the accuracy as a function of the multipole order, and as a function of the distance from the sphere centre to the wall. The problem of a freely moving sphere in these ambient flows is more complicated because of lubrication effects, caused by motion of the sphere with respect to the very close wall. Therefore in section 5, forces and torques on a sphere moving close to the wall in the absence of ambient flows are constructed by the pure multipole expansion, and alternatively, by a fast-convergent power-series expansion, applied after subtracting the lubrication asymptotic expressions, valid for very small gaps between the sphere surface and the wall. The accuracy of each method is estimated and the two are compared. In section 6, free motion of a sphere in ambient flows is evaluated and its precision is discussed, based on results from previous sections. Section 7 contains the final conclusions.

2. The problem

Three generic ambient flows parallel to a solid plane wall at $z = 0$ are considered:

$$\boldsymbol{u}_\infty = \begin{cases} k_{\mathrm{s}} z\, \boldsymbol{e}_x & \text{(pure shear)}, \\ k_{\mathrm{q}} z^2\, \boldsymbol{e}_x & \text{(quadratic)}, \\ 2k_{\mathrm{m}} zy\, \boldsymbol{e}_x & \text{(modulated shear)}, \end{cases} \tag{2.1}$$

with a solid sphere of radius a located at a distance ℓ from the wall; see Fig. 1. The same system was investigated in a companion paper (**20**) with the use of bipolar coordinates.

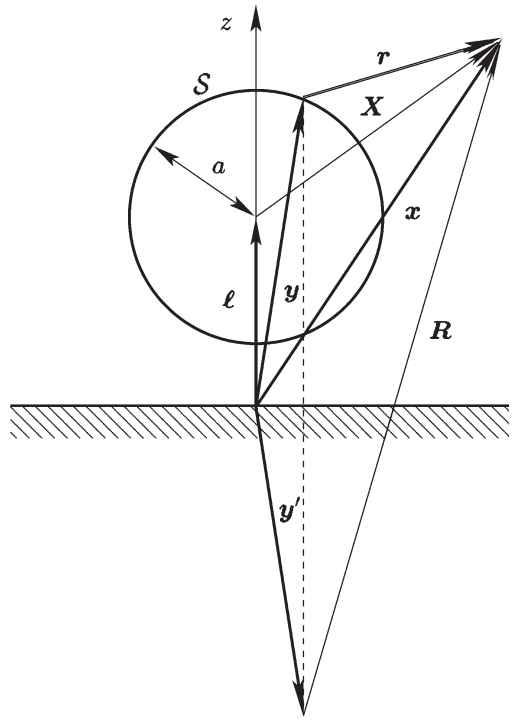

Fig. 1 Notation for a spherical particle close to a plane wall

Here another method will be applied: the multipole expansion. The ultimate goal is to estimate the accuracy of the multipole expansion in various physical contexts. Three generic problems will be solved, and precision of the following quantities will be estimated for a given multipole order:

(i) the force and torque exerted by the fluid on a motionless sphere in these ambient flows,
(ii) the force and torque exerted by the fluid on a sphere moving with given translational and angular velocities in the absence of ambient flow,
(iii) the translational and angular velocities of a freely moving sphere in these ambient flows.

The fluid velocity and pressure satisfy the Stokes equations, with the no-slip boundary conditions at the surfaces of the spheres and of the wall. The problem may be reformulated as a boundary integral equation (**13**, **14**) for the density of forces (the fluid normal stress) $[-\boldsymbol{\sigma}(\boldsymbol{y})\cdot\boldsymbol{n}_{\boldsymbol{y}}]$ induced at a point $\boldsymbol{y}$ on the sphere surface S (**21** to **23**), exerted by the sphere on the fluid,

$$\boldsymbol{U}+\boldsymbol{\Omega}\times(\boldsymbol{x}-\boldsymbol{\ell})=\boldsymbol{u}_\infty(\boldsymbol{x})-\int_{\mathcal{S}}\boldsymbol{G}(\boldsymbol{x},\boldsymbol{y})\cdot\boldsymbol{\sigma}(\boldsymbol{y})\cdot\boldsymbol{n}_{\boldsymbol{y}}\,dS_y,\quad \boldsymbol{x}\in\mathcal{S}. \tag{2.2}$$

Here $\boldsymbol{U}$ and $\boldsymbol{\Omega}$ denote the translational and angular velocities of the sphere, and $\boldsymbol{G}$ is the Green's function obtained by Blake (**15**) for velocity of the fluid bounded by a solid plane wall. Using the Cartesian indices $\alpha,\ \beta,\ \gamma=1,2,3$,

$$G_{\alpha\beta}(\boldsymbol{x},\boldsymbol{y})=T_{\alpha\beta}(\boldsymbol{r})-T_{\alpha\beta}(\boldsymbol{R})+2y_3(\delta_{\beta\gamma}-2\delta_{\beta3}\delta_{3\gamma})\frac{\partial}{\partial R_\gamma}\left[\frac{y_3R_\alpha}{8\pi\mu R^3}-T_{\alpha3}(\boldsymbol{R})\right], \tag{2.3}$$

Table 1 Definition of friction factors (see (2.1) and Fig. 1 for the notation)

Friction factor	Force divided by	Torque divided by	Ambient flow	Sphere
f^{s}_{xx}	$6\pi\,\mu\,a\ell k_{\mathrm{s}}$		pure shear	motionless
c^{s}_{yx}		$4\pi\,\mu\,a^3 k_{\mathrm{s}}$	pure shear	motionless
f^{q}_{xx}	$6\pi\,\mu\,a\ell^2 k_{\mathrm{q}}$		quadratic	motionless
c^{q}_{yx}		$8\pi\,\mu\,a^3\ell k_{\mathrm{q}}$	quadratic	motionless
c^{m}_{zx}		$-8\pi\,\mu\,a^3\ell k_{\mathrm{m}}$	modulated shear	motionless
f^{t}_{xx}	$-6\pi\,\mu\,aU$		no	translating with U along x
c^{t}_{yx}		$8\pi\,\mu\,a^2U$	no	translating with U along x
f^{r}_{xy}	$6\pi\,\mu\,a^2\Omega_y$		no	rotating with Ω_y along y
c^{r}_{yy}		$-8\pi\,\mu\,a^3\Omega_y$	no	rotating with Ω_y along y
c^{r}_{zz}		$-8\pi\,\mu\,a^3\Omega_z$	no	rotating with Ω_z along z

with $\boldsymbol{r} = (r_1, r_2, r_3) = \boldsymbol{x}-\boldsymbol{y}$, and $\boldsymbol{R} = (R_1, R_2, R_3) = \boldsymbol{x}-\boldsymbol{y}'$ where $\boldsymbol{y}'$ is symmetric to $\boldsymbol{y}$ with respect to the plane $z = 0$ (see Fig. 1). Further, δ is the Kronecker symbol, $y_3 = \boldsymbol{y}\cdot\boldsymbol{e}_z$, and $T_{\alpha\beta}$ denotes the Green's tensor for the unbounded fluid (the Oseen tensor), with

$$T_{\alpha\beta}(\boldsymbol{r}) = \frac{1}{8\pi\,\mu}\left(\frac{\delta_{\alpha\beta}}{r} + \frac{r_\alpha r_\beta}{r^3}\right), \tag{2.4}$$

where $r = |\boldsymbol{r}|$. The Green's function is symmetric, $G_{\alpha\beta}(\boldsymbol{x},\boldsymbol{y}) = G_{\beta\alpha}(\boldsymbol{y},\boldsymbol{x})$, as can be shown using the Lorentz reciprocity theorem (**14**).

In this paper, we follow the normalization used in the companion paper (**20**). The dimensionless forces and torques in the problems (i), (ii) are called *friction factors*. The normalization coefficients are listed in Table 1. They are chosen in such a way that for $\ell/a \to \infty$, the friction factors tend to unity (or zero). Translational velocities of the sphere in the problem (iii) are normalized by the corresponding values of the ambient flow at the sphere centre (and then denoted by $\tilde{U}$), and angular velocities by values of the ambient flow at the sphere centre divided by the sphere radius a (and then denoted by $\tilde{\Omega}$).

3. Multipole expansion

In (**20**, **24**), the solution to the problems (i), (ii) and (iii), specified in the previous section, has been determined in the bipolar coordinates as a linear combination of a large number of scalar harmonics. In this paper, we outline how to construct the solution as a linear combination of a large number of vector spherical harmonics (**25**, **26**), introduced to hydrodynamics of low-Reynolds-number flows by Felderhof (**23**).

Let us now summarize the irreducible multipole expansion (**18**, **27**). Following Cichocki and Jones (**16**), we apply this expansion to a single solid sphere in a fluid bounded by a planar solid

wall at $z = 0$, under a general ambient flow $\boldsymbol{u}_\infty(\boldsymbol{x})$. Note that the formulae given below are general and may also be applied to different geometries of the boundaries, if the corresponding Green's function is known. In this procedure, the forces, torques and velocities are projected on a basic set of multipole functions, and represented by the coefficients of this expansion (the so-called force and velocity multipoles); see Appendix A for details. Here we use the real multipole vector functions $\boldsymbol{u}^+_{lm\sigma}(\boldsymbol{X})$, with $\boldsymbol{X} = \boldsymbol{x} - \boldsymbol{\ell}$. The subscripts are the multipole indices $l = 1, 2, \ldots, m = 0, \pm 1, \ldots, \pm l$ and $\sigma = 0, 1, 2$. The definitions of all the $\boldsymbol{u}^+_{lm\sigma}(\boldsymbol{X})$ are given in (**7**) and some of the multipole functions are explicitly listed in Appendix B. The projection casts the integral equation (2.2) into an infinite set of algebraic equations, which relate the velocity multipoles $c(lm\sigma)$ to the force multipoles $f(l'm'\sigma')$ through known multipole matrix elements $M(lm\sigma, l'm'\sigma')$. For a fluid bounded by a solid plane wall, these matrix elements were determined in (**16**). One obtains

$$c(lm\sigma) = \sum_{l'=1}^{\infty} \sum_{m'=-l'}^{l'} \sum_{\sigma'=0}^{2} M(lm\sigma, l'm'\sigma')\ f(l'm'\sigma'), \tag{3.1}$$

where the force multipoles are defined as

$$f(lm\sigma) = -\int_S \boldsymbol{u}^+_{lm\sigma}(\boldsymbol{y} - \boldsymbol{\ell}) \cdot \boldsymbol{\sigma}(\boldsymbol{y}) \cdot \boldsymbol{n}_{\boldsymbol{y}}\, dS_{\boldsymbol{y}}. \tag{3.2}$$

The velocity multipoles $c(lm\sigma)$ contain the two contributions

$$c(lm\sigma) = c_0(lm\sigma) - c_\infty(lm\sigma), \tag{3.3}$$

which are the expansion coefficients of the velocity field $\boldsymbol{U} + \boldsymbol{\Omega} \times (\boldsymbol{y} - \boldsymbol{\ell})$ at a point $\boldsymbol{y}$ on the sphere surface (c_0), and of the velocity $\boldsymbol{u}_\infty(\boldsymbol{x})$ of the ambient flow at any point $\boldsymbol{x}$ of the fluid (c_∞). In other words,

$$\boldsymbol{U} + \boldsymbol{\Omega} \times (\boldsymbol{y} - \boldsymbol{\ell}) = \sum_{m=-1}^{1} \sum_{\sigma=0}^{1} c_0(1m\sigma)\ \boldsymbol{u}^+_{lm\sigma}(\boldsymbol{y} - \boldsymbol{\ell}), \tag{3.4}$$

$$\boldsymbol{u}_\infty(\boldsymbol{x}) = \sum_{l=1}^{\infty} \sum_{m=-l}^{l} \sum_{\sigma=0}^{2} c_\infty(lm\sigma)\ \boldsymbol{u}^+_{lm\sigma}(\boldsymbol{x} - \boldsymbol{\ell}). \tag{3.5}$$

Note that the only non-vanishing $c_0(lm\sigma)$ are those with $l = 1$, $\sigma = 0, 1$. Each of them is proportional to a component of the translational or the angular velocity of the sphere relative to the ambient flow. Similarly, the force multipoles with $(l, \sigma) = (1, 0)$ and $(l, \sigma) = (1, 1)$ are proportional to components of the force and the torque exerted by the fluid on the sphere, with coefficients given in Appendix A.

After truncating the expansion at multipole order L, that is, neglecting terms with $l, l' > L$, equation (3.1) reduces to a finite set of linear algebraic equations. These equations are solved for the force multipoles by inverting the large matrix $\mathbf{M}$ formed by the coefficients $M(lm\sigma, l'm'\sigma')$, with $l, l' \leqslant L$. More precisely, one obtains

$$f(lm\sigma) = \sum_{l'=1}^{L} \sum_{m'=-l'}^{l'} \sum_{\sigma'=0}^{2} Z_L(lm\sigma, l'm'\sigma')\ c(l'm'\sigma'), \tag{3.6}$$

where the so-called grand resistance (or generalized friction) matrix $\mathbf{Z}_L$ is the inverse of $\mathbf{M}$. Note that all coefficients $Z_L(lm\sigma, l'm'\sigma')$ depend on the choice of the truncation, that is, on the multipole

order L. For a single sphere immersed in a fluid bounded by a solid plane wall, $Z_L(lm\sigma, l'm'\sigma')$ has been calculated by Cichocki and Jones (**16**), using an algorithm based on the method of images and therefore similar to the approach of Schmitz and Felderhof (**27**) for two spheres in infinite fluid.

In the absence of an ambient flow, for given translational and angular velocities of the sphere (problem (ii) in section 2), the forces and the torques are determined by (3.6) with $l = 1$, $m = 0, \pm 1$ and $\sigma = 0, 1$,

$$f_{0,L}(1m\sigma) = \sum_{m'=-1}^{1} \sum_{\sigma'=0}^{1} Z_L(1m\sigma, 1m'\sigma')\, c_0(1m'\sigma'). \tag{3.7}$$

These multipole elements $Z_L(lm\sigma, l'm'\sigma')$, which enter (3.7), form the so-called *friction matrix*.

Let us now explain how the multipole expansion is applied to solve the problems (i) and (iii), introduced in section 2. We first project each ambient flow (that is, pure shear, quadratic and modulated shear) on to the basic set of the multipole functions. Each flow is a linear combination of several multipole vector functions with $l \leqslant 3$, listed in Appendix B (the corresponding coefficients $c_\infty(lm\sigma)$ can be deduced easily).

When the sphere is motionless in the ambient flow (problem (i) in section 2), we determine the force and torque exerted on the sphere. In the multipole expansion, this means that we search the force multipoles with $l = 1$, $m = 0, \pm 1$ and $\sigma = 0, 1$. We denote these as $f_{\infty,L}(1m\sigma)$, with the subscript ∞ specifying the problem (the sphere is fixed and the force multipoles are determined by all the coefficients $c_\infty(l'm'\sigma')$ only). Note that all the force multipoles depend on L, as indicated by the second subscript L. In particular, for pure shear and quadratic flows along $\boldsymbol{e}_x$, the forces (along $\boldsymbol{e}_x$) and the torques (along $\boldsymbol{e}_y$) are determined by $f_{\infty,L}(110)$ and $f_{\infty,L}(1\,{-}11)$, respectively. For the modulated shear flow, the force vanishes and the torque is perpendicular to the wall, that is, given by $f_{\infty,L}(101)$. These force multipoles are evaluated from (3.6), which takes the form

$$f_{\infty,L}(1m\sigma) = -\sum_{l'=1}^{L} \sum_{m'=-l'}^{l'} \sum_{\sigma'=0}^{2} Z_L(1m\sigma, l'm'\sigma')\, c_\infty(l'm'\sigma'). \tag{3.8}$$

Note that in precise computations, the selected multipole order L should be large enough to include in the above sum all the coefficients $c_\infty(l'm'\sigma') \neq 0$. In Appendix C, equation (3.8) is expressed in terms of friction factors rather than $f_{\infty,L}$, with the use of Table 1 and Appendix A.

When the sphere is freely moving in an ambient flow, with $f(lm\sigma) = 0$ for $l = 1$, $m = 0, \pm 1$ and $\sigma = 0, 1$, then the goal is to determine its translational and rotational velocities (problem (iii) in section 2). These velocities are expressed by the velocity multipoles with $l = 1$, $m = 0, \pm 1$ and $\sigma = 0, 1$, as in Appendix A. By virtue of (3.3) and (3.6), one obtains

$$c_{0,L}(1m\sigma) = -\sum_{m'=-1}^{1} \sum_{\sigma'=0}^{1} \mu_L(1m\sigma, 1m'\sigma')\; f_{\infty,L}(1m'\sigma'), \tag{3.9}$$

with $f_{\infty,L}$ already calculated in (3.8). Here $\mu_L(lm\sigma, l'm'\sigma')$ denote coefficients of the 6×6 *mobility matrix*, which is the inverse of the corresponding 6×6 friction matrix,

$$\begin{pmatrix} \tilde{U}^{\mathrm{s}} \\ \tilde{\Omega}^{\mathrm{s}} \end{pmatrix} = \begin{pmatrix} f^{\mathrm{t}}_{xx} & -\frac{4}{3}c^{\mathrm{t}}_{yx} \\ -\frac{4}{3}c^{\mathrm{t}}_{yx} & \frac{4}{3}c^{\mathrm{r}}_{yy} \end{pmatrix}^{-1} \begin{pmatrix} \ell/a\; f^{\mathrm{s}}_{xx} \\ \frac{2}{3}\, c^{\mathrm{s}}_{yx} \end{pmatrix}, \tag{3.10}$$

$$\begin{pmatrix} \tilde{U}^{\mathrm{q}} \\ \tilde{\Omega}^{\mathrm{q}} \end{pmatrix} = \begin{pmatrix} f^{\mathrm{t}}_{xx} & -\frac{4}{3}c^{\mathrm{t}}_{yx} \\ -\frac{4}{3}c^{\mathrm{t}}_{yx} & \frac{4}{3}c^{\mathrm{r}}_{yy} \end{pmatrix}^{-1} \begin{pmatrix} (\ell/a)^2\ f^{\mathrm{q}}_{xx} \\ \frac{4}{3}\ \ell/a\ c^{\mathrm{q}}_{yx} \end{pmatrix}, \tag{3.11}$$

$$\tilde{\Omega}^{\mathrm{m}} = (c^{\mathrm{r}}_{zz})^{-1}\ c^{\mathrm{m}}_{zx}, \tag{3.12}$$

where Table 1 and Appendix A have been used.

The algorithm described above has been implemented in a numerical FORTRAN code and calculations have been carried out with quadruple precision (32 digits). The accuracy will be discussed in the following sections.

4. Motionless sphere in an ambient flow

In this section, equation (3.8) is applied to compute the forces and torques exerted on a single sphere by pure shear, quadratic, and modulated shear ambient flows. The accuracy is estimated numerically by analysing the forces and torques as functions of the multipole order L.

Challenged by the precise (truncated at 16 digits) results of Pasol *et al.* (**20**), we start by asking whether it is possible to obtain such a high accuracy also from the multipole expansion. First, we consider the forces and torques applied by the quadratic ambient flow. Using (C.8) and (C.9) from Appendix C, we calculate the corresponding friction factors, that is, $f^{\mathrm{q}}_{xx}(L)$ and $c^{\mathrm{q}}_{yx}(L)$, as functions of L. Next, we construct a sequence of the differences, $b_L = \mathcal{F}(L) - \mathcal{F}(L-1)$, with $\mathcal{F}$ equal to f^{q}_{xx} or c^{q}_{yx}. As illustrated in Fig. 2, for large L the following inequalities are numerically observed:

$$|b_L| \leqslant \begin{cases} \dfrac{c}{L^4} & \text{for } \ell/a \leqslant 1{\cdot}0001, \\ b\,q^L & \text{for } \ell/a \geqslant 1{\cdot}001, \end{cases} \tag{4.1}$$

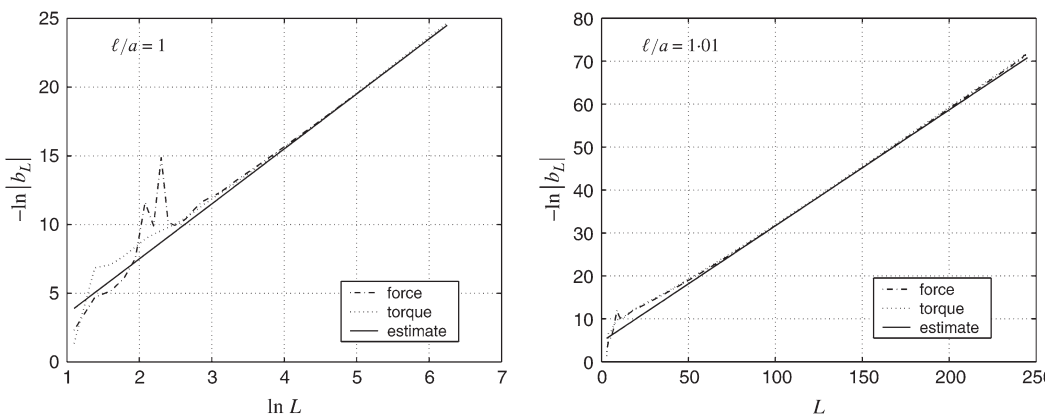

Fig. 2 A fixed sphere in a quadratic ambient flow: convergence rate of the multipole expansion. For the force, $b_L = f^{\mathrm{q}}_{xx}(L) - f^{\mathrm{q}}_{xx}(L-1)$, and for the torque, $b_L = c^{\mathrm{q}}_{yx}(L) - c^{\mathrm{q}}_{yx}(L-1)$, where L is the multipole order. For $\ell/a \leqslant 1{\cdot}0001$ (left plot with $\ell/a = 1$), b_L is estimated by c/L^4 whereas for $\ell/a \geqslant 1{\cdot}001$ (the right plot with $\ell/a = 1{\cdot}01$), b_L is estimated by bq^L

where c is constant and b, q depend on ℓ/a. The uncertainty of a friction factor $\mathcal{F}(L)$ is thus estimated as follows:

$$|\mathcal{F}(L) - \mathcal{F}(\infty)| = \left| \sum_{l=L+1}^{\infty} b_l \right| \leqslant \begin{cases} \dfrac{c}{3L^3} & \text{for } \ell/a \leqslant 1{\cdot}0001, \\ \dfrac{b\, q^{L+1}}{1-q} & \text{for } \ell/a \geqslant 1{\cdot}001. \end{cases} \tag{4.2}$$

The change of the scaling at intermediate distances between $\ell/a = 1{\cdot}0001$ and $\ell/a = 1{\cdot}001$ is related to the rapid increase of accuracy for $\ell/a \geqslant 1{\cdot}001$.

If the sphere is far from the wall, then the scaling $b_L \sim (a/\ell)^{2L}$ can be derived from the multiple scattering expansion. For small distances, however, b_L is a complicated function of L and ℓ/a. The characteristic size of the gap corresponding to transition from exponential to algebraic convergence, and the specific scaling $1/L^4$ law are just the numerical findings, which would require further theoretical explanation.

For $\ell/a \leqslant 1{\cdot}0001$, we improve the 5×10^{-9} accuracy deduced from (4.2). This has been achieved by extrapolating the results from a finite to an infinite multipole order, as illustrated in Fig. 3. From (4.2) it follows that for small distances, $|f^{\mathrm{q}}_{xx}(L) - f^{\mathrm{q}}_{xx}(\infty)| \sim 1/L^3$ and we therefore plot $f^{\mathrm{q}}_{xx}(L)$ versus $1/L^3$. For very small ℓ/a, $f^{\mathrm{q}}_{xx}(L)$ and $c^{q}_{yx}(L)$ are decreasing functions of L (for $L \geqslant 10$ and $L \geqslant 3$, respectively). By extrapolating the line to $1/L^3 \to 0$ we thus obtain the corrected value $f^{\mathrm{q}}_{xx}(\infty)$. A similar extrapolation has been carried out for the torque. The corresponding estimate of the multipole precision is listed in Table 2.

For $\ell/a \geqslant 1{\cdot}001$, the convergence with L is fast and we may decrease the multipole order below 500 to keep the 5×10^{-17} accuracy, chosen in the companion paper (**20**). The multipole order L sufficient to keep this precision is evaluated and listed in Table 2. Instead of applying (4.2), it is

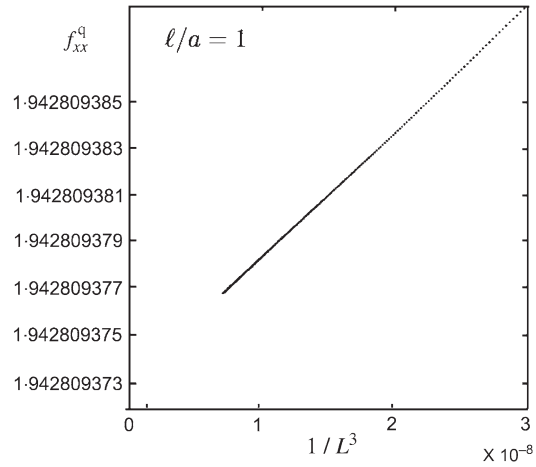

Fig. 3 The dimensionless force f^{q}_{xx} on a sphere fixed at $\ell/a = 1$ in a quadratic ambient flow versus $1/L^3$. Extrapolation of the plot with a straight line from a finite to the infinite multipole order L results in more accurate value of f^{q}_{xx}

Table 2 The multipole order L needed to obtain the indicated absolute precision of the dimensionless forces and torques f^{s}_{xx}, c^{s}_{yx}, f^{q}_{xx}, c^{q}_{yx}, and c^{m}_{zx}, exerted on a fixed sphere centred at a distance ℓ from the wall by pure shear, quadratic, and modulated shear flows, respectively

	f^{s}_{xx}, c^{s}_{xx}		f^{q}_{xx}, c^{q}_{xx}		c^{m}_{zx}	
ℓ/a	L	precision	L	precision	L	precision
1·0	500	5×10^{-10}	500	5×10^{-10}	92	5×10^{-17}
1·000002	500	5×10^{-10}	500	5×10^{-10}	92	5×10^{-17}
1·000005	500	1×10^{-9}	500	5×10^{-10}	92	5×10^{-17}
1·00001	500	1×10^{-9}	500	1×10^{-9}	92	5×10^{-17}
1·0001	500	5×10^{-10}	500	1×10^{-9}	91	5×10^{-17}
1·001	373,378	5×10^{-17}	381,377	5×10^{-17}	79	5×10^{-17}
1·005	174,175	5×10^{-17}	177,176	5×10^{-17}	66	5×10^{-17}
1·01	124,126	5×10^{-17}	127,126	5×10^{-17}	60	5×10^{-17}
1·05	56	5×10^{-17}	57	5×10^{-17}	38	5×10^{-17}
1·1	40,41	5×10^{-17}	39,40	5×10^{-17}	30	5×10^{-17}
1·2	29,30	5×10^{-17}	28	5×10^{-17}	24	5×10^{-17}
1·5	20	5×10^{-17}	18	5×10^{-17}	16	5×10^{-17}
2·0	14	5×10^{-17}	13,14	5×10^{-17}	12	5×10^{-17}
4·0	9	5×10^{-17}	9	5×10^{-17}	7	5×10^{-17}
5·0	8	5×10^{-17}	8	5×10^{-17}	6	5×10^{-17}
10·0	6	5×10^{-17}	6	5×10^{-17}	4	5×10^{-17}
21·0	5	5×10^{-17}	5	5×10^{-17}	3	5×10^{-17}
51·0	4	5×10^{-17}	4	5×10^{-17}	2	5×10^{-17}

equivalent to look at the smallest L at which the sixteenth digit after the decimal point does not change any more if the multipole order is increased.

In pure shear ambient flow, the forces and the torques $f^{s}_{xx}(L)$ and $c^{s}_{yx}(L)$ scale with L also according to (4.2). Moreover, they are increasing functions of L, if $L \geqslant 7$ and $L \geqslant 2$, respectively. Therefore, for $\ell/a \leqslant 1{\cdot}0001$ the forces and torques due to pure shear are extrapolated in the same way as in case of quadratic flow. The multipole precision is listed in Table 2, together with the multipole order L sufficient to keep the 5×10^{-17} precision for $\ell/a \geqslant 1{\cdot}001$.

The calculation of the torque exerted on the motionless sphere in the modulated shear ambient flow is significantly more precise than the evaluation of the friction factors in the quadratic flow. Even at contact, we obtain the exact result of Goren and O'Neill (**28**), that is, $\pi^4/90$, with a 32-digit precision. To keep the chosen 5×10^{-17} accuracy at any value of ℓ/a, we need significantly less multipoles than in the case of quadratic flow, as indicated by the corresponding values of L in Table 2.

Table 2 allows for an easy comparison with the results obtained in bipolar coordinates (**20**, **24**). Our accuracy is lower only for the pure shear and quadratic friction factors, and only for $1 \leqslant \ell/a \leqslant 1{\cdot}0001$. In this case, the maximal multipole precision is 10^{-10} to 10^{-9} (in bipolar coordinates, 5×10^{-17} for $1 < \ell/a \leqslant 1{\cdot}0001$ and 5×10^{-11} for $\ell/a = 1$). Within the estimated precision, all our values of the forces and the torques coincide with those obtained in bipolar coordinates (**20**, **24**).

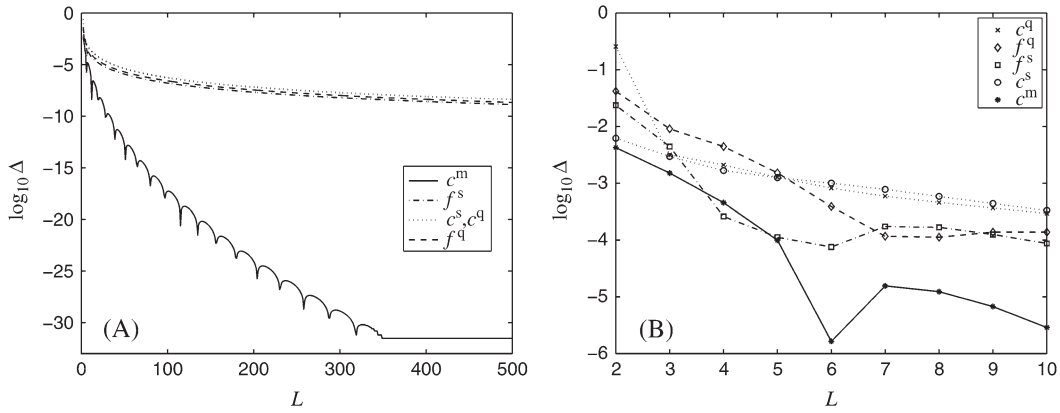

Fig. 4 Relative accuracy $\Delta = |\mathcal{F}(L) - \mathcal{F}(500)|/\mathcal{F}(500)$ of the friction factors $\mathcal{F}(L)$ as functions of the multipole order L. The sphere is at contact with the wall, $\ell/a = 1$. (A): the whole range of multipole orders L. (B): small L only

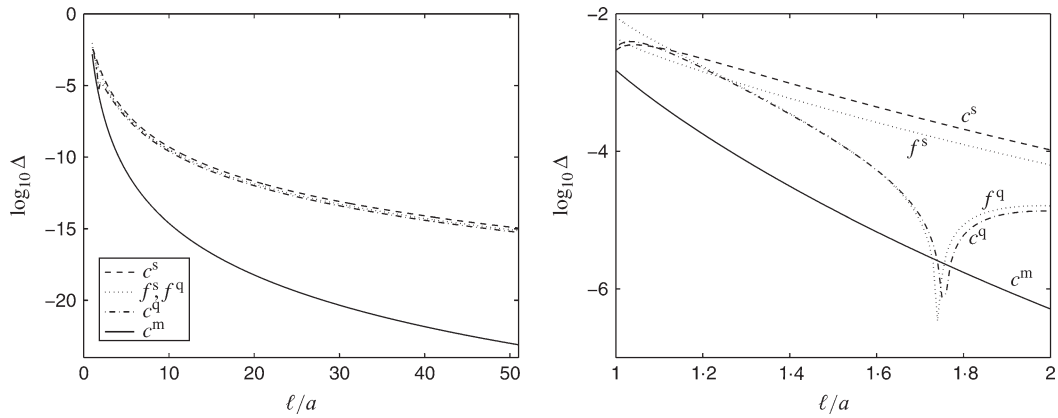

Fig. 5 Relative accuracy $\Delta = |\mathcal{F}(L) - \mathcal{F}(100)|/\mathcal{F}(100)$ of the friction factors $\mathcal{F}(L)$ as functions of the distance ℓ/a between the sphere centre and the wall. The multipole order $L = 3$. Left: large and small ℓ/a. Right: small ℓ/a only

Now we focus on a sphere at contact with the wall. We compare relative accuracy of the friction factors for different ambient flows.[†] In Fig. 4A, the resulting relative accuracy is plotted as a function of the multipole order $3 \leqslant L \leqslant 500$.

For practical applications, it is especially important to analyse the relative accuracy for very low values of the multipole order L. From Fig. 4B it follows that $L = 3$ is already sufficient to

[†] For large ℓ/a, the friction factors tend to 1. For smaller distances, they are also $\mathcal{O}(1)$. At $\ell/a = 1$, $f^{\mathrm{s}}_{xx} = 1{\cdot}7006182335$, $c^{\mathrm{s}}_{yx} = 0{\cdot}943986501$, $f^{\mathrm{q}}_{xx} = 1{\cdot}942809373$, $c^{\mathrm{q}}_{yx} = 0{\cdot}990770518$, and $c^{\mathrm{m}}_{zx} = \pi^4/90$.

obtain one per cent relative accuracy of the forces and torques on the sphere at contact with the wall. Indeed, for the motionless sphere, there is no lubrication effect, and fast convergence of the multipole expansion has been expected even at the contact, where the accuracy is the lowest. The last conclusion is clearly seen in Fig. 5, where the relative accuracy of the forces and torques, calculated with $L = 3$, is plotted versus ℓ/a. Therefore $L = 3$ is sufficient to obtain one per cent relative accuracy for arbitrary separations between the sphere surface and the wall.

5. Moving sphere, no ambient flow

In this section, we focus on the friction factors f^{t}_{xx}, c^{t}_{yx} and c^{r}_{yy} and their accuracy.

5.1 *Pure multipole expansion*

For large and intermediate distances, $\ell/a \geqslant 1{\cdot}001$, we evaluate the friction factors $\mathcal{F}(L)$, equal to $f^{\mathrm{t}}_{xx}(L)$, $c^{\mathrm{t}}_{yx}(L)$ and $c^{\mathrm{r}}_{yy}(L)$, as functions of the multipole order L. We estimate the (absolute) precision in the same way as previously, since we also obtain $|b_L| \leqslant bq^L$ in this range. The top accuracy of $f^{\mathrm{t}}_{xx}(L)$, $c^{\mathrm{t}}_{yx}(L)$ and $c^{\mathrm{r}}_{yy}(L)$ is comparable to that of $f^{\mathrm{q}}_{xx}(L)$ and $c^{\mathrm{q}}_{yx}(L)$, but more multipoles are needed to reach the same precision. Results are listed in Table 3.

If a solid sphere moves with respect to a close solid wall, lubrication forces dominate and the multipole expansion of the friction factors f^{t}_{xx}, c^{t}_{yx} and c^{r}_{yy} converges very slowly. For example, at $\ell/a = 1{\cdot}001$, the 0·01 absolute precision is reached for as many as $L \sim 90$. For small distances, the previous estimate (4.1) is now replaced by $|b_L| \leqslant d/L$. Indeed, for $\ell/a \to 1$, values of the friction factors diverge, and their uncertainty rapidly increases. There is no analogue of Fig. 3. For $\ell/a \leqslant 1{\cdot}0001$, we use a more accurate method (called in brief a 'power series'), proposed by Cichocki and Jones (**16**). In this range, even for $L = 500$, absolute precision of the pure multipole expansion is poor in comparison to the power-series accuracy. Therefore the absolute precision of the pure multipole expansion is evaluated as the difference between the multipole-expansion values and the power-series values of the friction factors, and listed in Table 3.

5.2 *Power series*

Making the inverse-power-series expansion in ℓ/a of the friction factors $\mathcal{F} = f^{\mathrm{t}}_{xx}$, c^{t}_{yx} and c^{r}_{yy}, it is essential to speed up the convergence rate by subtracting the corresponding asymptotic expressions, non-analytical and divergent at close distances (**29**). For a single sphere next to a flat hard wall, such a procedure has been constructed by Cichocki and Jones (**16**). They used the multipole expansion to evaluate

$$\mathcal{G} = \mathcal{F} - (A \ln \xi + B\, \xi \ln \xi), \tag{5.1}$$

with $\xi = \ell/a - 1$, and A, B listed in (**16**). Then, they expanded the difference $\mathcal{G}$ in the inverse powers of ℓ/a, and truncated at a certain large power n,

$$\mathcal{G}(n) = \sum_{k=0}^{n} D_k \left(\frac{a}{\ell}\right)^k. \tag{5.2}$$

The idea originates from Jeffrey and Onishi (**29**), who considered two unequal spheres in infinite space. In the limit of infinite radius of sphere 2 (which becomes the plane wall), the Jeffrey–Onishi functions Y^A_{11}, Y^B_{11} and Y^C_{11} tend to f^{t}_{xx}, $-2\, c^{\mathrm{t}}_{yx}$ and c^{r}_{yy}, respectively.

Table 3 Absolute precision of friction factors f^{t}_{xx}, c^{t}_{yx} and c^{r}_{yy}, as calculated by the power series and, alternatively, by the pure multipole expansion. The power n and the multipole order L sufficient to obtain this precision are indicated

					absolute precision					
		L			f^{t}_{xx}		c^{t}_{yx}		c^{r}_{yy}	
ℓ/a	n	f^{t}_{xx}	c^{t}_{yx}	c^{r}_{yy}	power series	pure multipole	power series	pure multipole	power series	pure multipole
1·000002	450	500	500	500	5×10^{-9}	0·56	2×10^{-8}	0·13	5×10^{-8}	0·44
1·000005	450	500	500	500	5×10^{-9}	0·27	2×10^{-8}	0·12	5×10^{-8}	0·22
1·00001	450	500	500	500	5×10^{-9}	0·13	2×10^{-8}	8×10^{-2}	1×10^{-7}	0·10
1·0001	450	500	500	500	5×10^{-9}	3×10^{-4}	2×10^{-8}	3×10^{-4}	1×10^{-7}	3×10^{-4}
1·001	450	500	500	500	5×10^{-9}	7×10^{-16}	3×10^{-8}	5×10^{-16}	1×10^{-7}	5×10^{-16}
1·005	450	230	225	225	5×10^{-9}	5×10^{-17}	1×10^{-8}	5×10^{-17}	1×10^{-7}	5×10^{-17}
1·01	450	160	155	160	5×10^{-10}	5×10^{-17}	5×10^{-9}	5×10^{-17}	2×10^{-8}	5×10^{-17}
1·05	450	70	70	70	5×10^{-17}	5×10^{-17}	5×10^{-17}	5×10^{-17}	5×10^{-17}	5×10^{-17}
1·1	295	46	49	45	5×10^{-17}	5×10^{-17}	5×10^{-17}	5×10^{-17}	5×10^{-17}	5×10^{-17}
1·2	160	32	35	32	5×10^{-17}	5×10^{-17}	5×10^{-17}	5×10^{-17}	5×10^{-17}	5×10^{-17}
1·5	75	21	20	21	5×10^{-17}	5×10^{-17}	5×10^{-17}	5×10^{-17}	5×10^{-17}	5×10^{-17}
2·0	46	16	13	15	5×10^{-17}	5×10^{-17}	5×10^{-17}	5×10^{-17}	5×10^{-17}	5×10^{-17}
4·0	23	9	9	9	5×10^{-17}	5×10^{-17}	5×10^{-17}	5×10^{-17}	5×10^{-17}	5×10^{-17}
5·0	20	8	8	7	5×10^{-17}	5×10^{-17}	5×10^{-17}	5×10^{-17}	5×10^{-17}	5×10^{-17}
10·0	14	6	6	5	5×10^{-17}	5×10^{-17}	5×10^{-17}	5×10^{-17}	5×10^{-17}	5×10^{-17}
21·0	11	5	5	4	5×10^{-17}	5×10^{-17}	5×10^{-17}	5×10^{-17}	5×10^{-17}	5×10^{-17}
51·0	9	4	3	3	5×10^{-17}	5×10^{-17}	5×10^{-17}	5×10^{-17}	5×10^{-17}	5×10^{-17}

In (**16**), the power-series expansion of $\mathcal{F}$ was constructed from the multipole expansion, represented as a sum of multiple scatterings. Then, subtracting the power-series expansion of the lubrication expressions $A\ln\xi + B\,\xi\ln\xi$, they obtained a fast-convergent series $\mathcal{G}$. The lubrication asymptotics is essential to determine D_k as a function of k. Indeed, if $\xi \to 0$, then $\mathcal{G} = \mathcal{O}(\xi^2 \log\xi)$, and therefore $D_k = \mathcal{O}(1/k^3)$. However, for c^{r}_{yy}, f^{t}_{xx} and c^{t}_{yx}, this scaling cannot be directly used to estimate the truncation error, because of large oscillations inherent to the inverse-power expansion in ℓ/a, illustrated in Fig. 6A. We thus use a procedure equivalent to that introduced in (**16**), that is, we represent the term $\mathcal{G}$ as $\mathcal{G}^{(p)}(n) = [\mathcal{G}^{(p-1)}(n) + \mathcal{G}^{(p-1)}(n-1)]/2$, with $\mathcal{G}^{(0)}(n) = \mathcal{G}(n)$. With $p = 3$, we then decrease amplitude of the oscillations by two orders of magnitude, as shown in

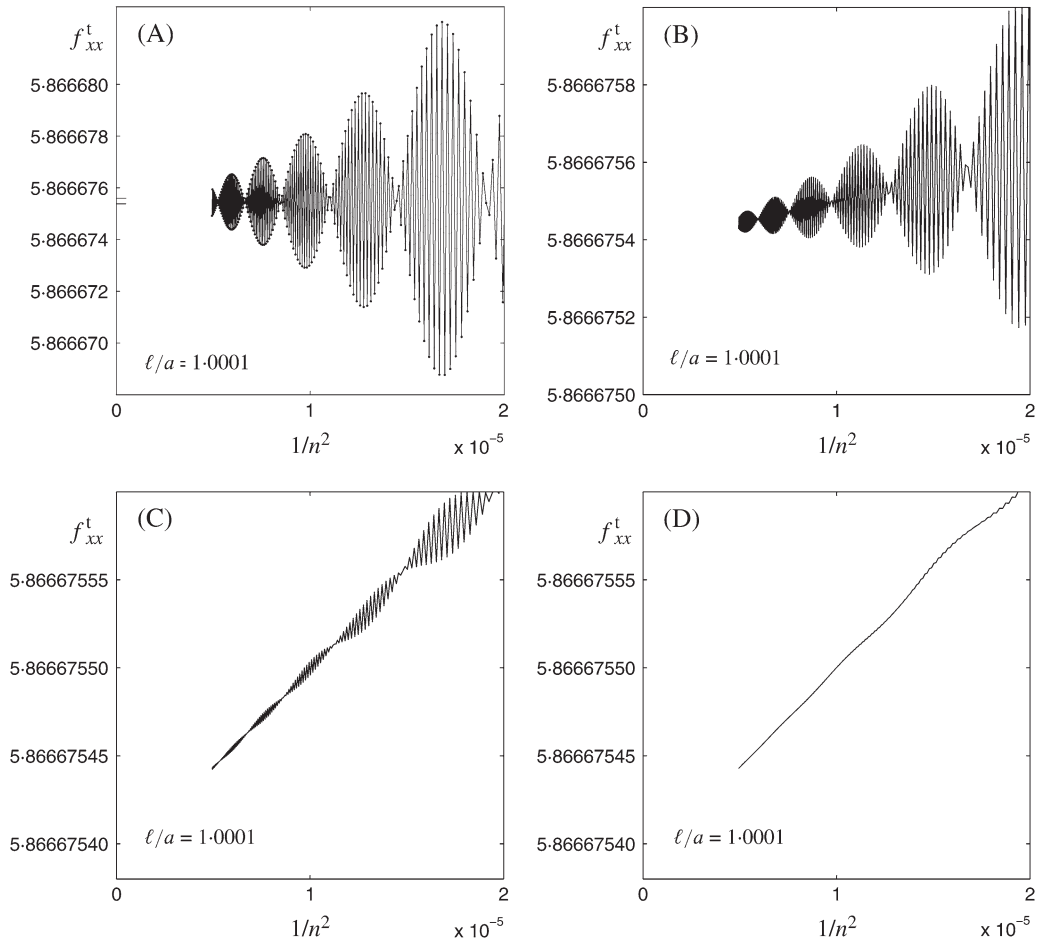

Fig. 6 The friction coefficient f^{t}_{xx} versus $1/n^2$, calculated from (5.1) with (A) $\mathcal{G}(n)$; (B) $\mathcal{G}^{(1)}(n)$; (C) $\mathcal{G}^{(2)}(n)$; (D) $\mathcal{G}^{(3)}(n)$. Extrapolation of plot (D) to $1/L = 0$ with a straight line finally results in $f^{\mathrm{t}}_{xx} = 5{\cdot}86667539 \pm 5 \times 10^{-9}$. To illustrate the improved accuracy, we have marked on the vertical axis of plot (A) two small ticks, which correspond to the range of ordinates in plot (D)

Fig. 6D. For very small ℓ/a, almost linear dependence of the friction factors on $1/n^2$ is obtained, consistently with $D_k = \mathcal{O}(1/k^3)$. For $\ell/a \leqslant 1{\cdot}01$, we extrapolate values of the friction factors from $n = 450$ to $n = \infty$, as illustrated in Fig. 6, improving precision of (**16**). Precision of the extrapolated values is listed in Table 3 as the 'absolute precision of the power series'.

It is important to mention that the extrapolation correction can be deduced from the lubrication expansion. For ℓ/a close to one, Chaoui and Feuillebois (**24**) determined the asymptotic lubrication expansion of the friction factors up to $\mathcal{O}(\xi^5 \log \xi)$. In particular, they evaluated $C\,\xi^2 \log \xi$, with $C \approx 0{\cdot}0116$ for f^{t}_{xx}, $C \approx -0{\cdot}0369$ for c^{t}_{yx}, and $C \approx -0{\cdot}213$ for c^{r}_{yy}. Expanding $C\,\xi^2 \log \xi$ in powers of a/ℓ, we evaluate the extrapolation correction as

$$-2C \sum_{k=n+1}^{\infty} \frac{1}{k^3} \left(\frac{a}{\ell}\right)^k. \tag{5.3}$$

Indeed, (5.3) is in excellent quantitative agreement with our extrapolation correction.

Actually, (5.3) can be used to estimate and improve precision of the power series not only for very small, but also for larger distances. The point is that $\mathcal{G}^{(3)}$ practically do not oscillate, and $\mathcal{F}^{(3)}(n) = \mathcal{G}^{(3)}(n) + A \ln \xi + B\,\xi \ln \xi$ are linear functions of $S(n) = \sum_{k=n+1}^{\infty} (a/\ell)^k/k^3$. The reference variable $S(n)$ is a straightforward generalization of $1/n^2$ used in Fig. 6. For $\ell/a = 1{\cdot}05$, the linear dependence of $\mathcal{F}^{(3)}(n)$ on $S(n)$ is illustrated in Fig. 7. The slopes of the straight lines in Fig. 7 correspond to $2C = 0{\cdot}025$ for f^{t}_{xx}, $2C = -0{\cdot}08$ for c^{t}_{yx}, $2C = -0{\cdot}46$ for c^{r}_{yy}, in agreement with the corresponding values calculated in (**24**). The friction factor c^{r}_{zz} has also been plotted in the same figure, with $2C = 0{\cdot}9$. This is the only friction factor finite at the contact, with $c^{\mathrm{r}}_{zz} = \zeta(3) \approx 1{\cdot}202057$.

For practical purposes, very high accuracy is not needed. In Fig. 8, absolute precision of the power series is studied as a function of the truncation power n. Here $\ell/a = 1$ is taken, where

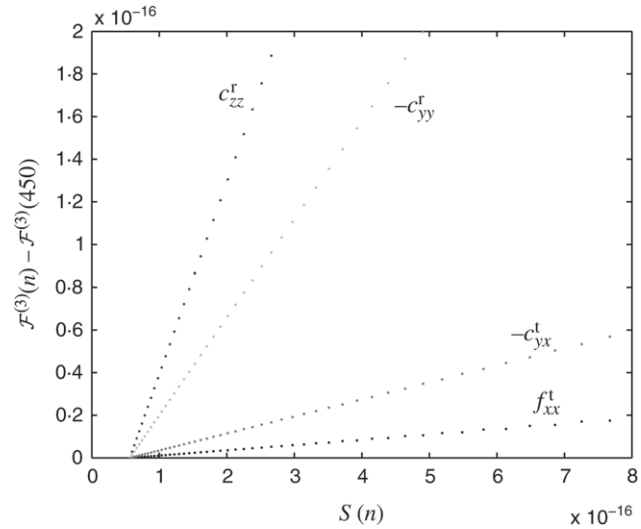

Fig. 7 Friction factors $\mathcal{F}^{(3)}(n) = c^{\mathrm{r}}_{zz},\ c^{\mathrm{r}}_{yy},\ c^{\mathrm{t}}_{yx},\ f^{\mathrm{t}}_{xx}$ as a function of $S(n) = \sum_{k=n+1}^{\infty} (a/\ell)^k/k^3$, for $\ell/a = 1{\cdot}05$. The upper limit in the sum is numerically approximated by 10000

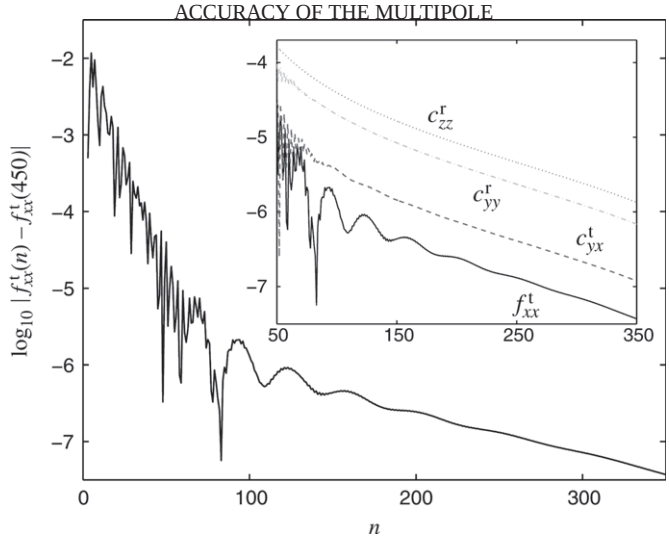

Fig. 8 Absolute precision of the friction factor f^{t}_{xx} versus the power n of the series truncation. Here $\ell/a = 1$. Inset: analogical plots for the friction factors c^{r}_{zz}, c^{r}_{yy}, c^{t}_{yx} and f^{t}_{xx}

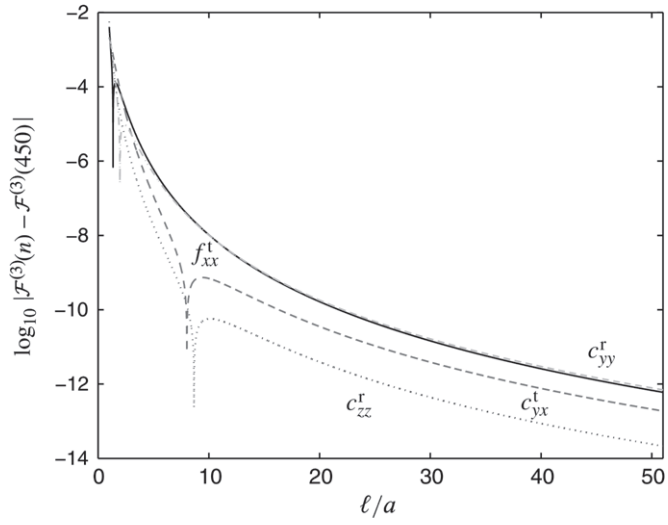

Fig. 9 Absolute precision of the friction factors $\mathcal{F} = c^{\mathrm{r}}_{zz},\ c^{\mathrm{r}}_{yy},\ c^{\mathrm{t}}_{yx},\ f^{\mathrm{t}}_{xx}$ versus the distance ℓ/a between the sphere centre and the wall. The series is truncated at $n = 8$

the convergence rate is the slowest. Figure 9 illustrates how the absolute precision changes with distance from the wall. The truncation power as small as $n = 8$ is sufficient to reach the one per cent absolute precision for all the distances. The 'cusps' seen in Fig. 9 correspond to intersections of curves $\mathcal{F}^{(3)}(n)$ and $\mathcal{F}^{(3)}(450)$ for some values of ℓ/a.

5.3 *Comparison*

In summary, the friction factors f^{t}_{xx}, c^{t}_{yx} and c^{r}_{yy} and their accuracy have been calculated by two methods. In Table 3, we list the 'top precision' of the pure multipole expansion, and of the inverse-power expansion in ℓ/a. For $\ell/a \geqslant 1{\cdot}05$, we reach by both methods the chosen 5×10^{-17} accuracy with powers L and n of the corresponding truncations listed in Table 3. For $\ell/a \leqslant 1{\cdot}01$, the convergence of the power expansion slows down and the precision rapidly deteriorates because we numerically cannot go beyond $n = 450$. As a result, in the range of $1{\cdot}001 \leqslant \ell/a \leqslant 1{\cdot}01$, the multipole expansion is slightly more accurate than the power series. For very close distances $\ell/a \leqslant 1{\cdot}001$, it is essential to take into account the lubrication effects, therefore in this range the pure multipole expansion is practically of no use. Within the specified accuracy, values of the friction factors f^{t}_{xx}, c^{t}_{yx} and c^{r}_{yy} calculated here (and listed in table D1 in Appendix D) coincide with the results obtained in bipolar coordinates (**24**).

It is important to stress that for a single sphere close to a wall, the inverse-power expansion is more practical (convenient and faster) than the pure multipole expansion, because the expansion coefficients are calculated only once for all the separations. For many spheres, however, the most efficient method is the multipole expansion with a low multipole order, combined with pairwise sphere–sphere and sphere–wall lubrication corrections, each built from a corresponding power series, truncated at a large power n.

6. Freely moving sphere in an ambient flow

Free motion of a sphere immersed in pure shear and quadratic flows has been calculated with a high precision from (3.10), (3.11). The 'top relative accuracy' of the translational and angular sphere velocities, listed in Table 4, has been evaluated in the standard way from the 'top absolute precision' of the corresponding friction factors. Within this accuracy, our values coincide with the results obtained in bipolar coordinates in (**20**, **24**). For $n = 450$ and a small multipole order $L = 3$, in the whole range of the distances, the relative accuracy of the translational and angular sphere velocities coincides with that of the corresponding friction factors; see Fig. 5.

Table 4 Top relative accuracy of the translational and angular velocities, $\tilde{U}^{\mathrm{s}}$, $\tilde{\Omega}^{\mathrm{s}}$, $\tilde{U}^{\mathrm{q}}$ and $\tilde{\Omega}^{\mathrm{q}}$ of a sphere with its centre at a distance ℓ from the wall, freely moving in an ambient pure shear and a quadratic flow, respectively. For $\ell/a \geqslant 1{\cdot}005$, the chosen accuracy 5×10^{-17} is easily obtained

	relative accuracy of			
ℓ/a	$\tilde{U}^{\mathrm{s}}$	$\tilde{\Omega}^{\mathrm{s}}$	$\tilde{U}^{\mathrm{q}}$	$\tilde{\Omega}^{\mathrm{q}}$
1·000002	3×10^{-9}	1×10^{-8}	4×10^{-9}	1×10^{-8}
1·000005	3×10^{-9}	1×10^{-8}	4×10^{-9}	1×10^{-8}
1·00001	4×10^{-9}	2×10^{-8}	5×10^{-9}	2×10^{-8}
1·0001	4×10^{-9}	3×10^{-8}	6×10^{-9}	3×10^{-8}
1·001	2×10^{-16}	4×10^{-16}	2×10^{-16}	3×10^{-16}

The translational and angular sphere velocities decrease to zero when the sphere tends to touch the wall. However, there appears a non-vanishing slip $\tilde{\Omega}_y^{\mathrm{s,q}}/\tilde{U}^{\mathrm{s,q}}$ in this limit. Using (3.10), (3.11), and the relations (C.11) given in (**30**, **31**), we obtain at the contact

$$\frac{\tilde{\Omega}_y^{\mathrm{s}}}{\tilde{U}^{\mathrm{s}}} = \frac{8c_{yx}^{\mathrm{s}} + 3\,f_{xx}^{\mathrm{s}}}{2(c_{yx}^{\mathrm{s}} + 6\,f_{xx}^{\mathrm{s}})} \qquad \text{and} \qquad \frac{\tilde{\Omega}_y^{\mathrm{q}}}{\tilde{U}^{\mathrm{q}}} = \frac{16c_{yx}^{\mathrm{q}} + 3\,f_{xx}^{\mathrm{q}}}{4(c_{yx}^{\mathrm{q}} + 3\,f_{xx}^{\mathrm{q}})}. \tag{6.1}$$

With the calculated values of $f_{xx}^{\mathrm{s,q}}$ and $c_{yx}^{\mathrm{s,q}}$, we obtain $\tilde{\Omega}_y^{\mathrm{s}}/\tilde{U}^{\mathrm{s}} = 0{\cdot}567549869$ (improving the precision of (**32**)), and $\tilde{\Omega}_y^{\mathrm{q}}/\tilde{U}^{\mathrm{q}} = 0{\cdot}794842531$. In pure shear flow, the slip at the contact is more significant than in quadratic flow.

7. Conclusions

A single sphere near a plane wall in quadratic and pure shear low-Reynolds-number flows has been considered. The force and the torque exerted on the motionless sphere by the fluid were evaluated by a multipole expansion. The same method has been applied to determine the free motion of the sphere. For very small separations $\ell/a - 1 \leqslant 10^{-4}$ between the sphere surface and the wall, the 'top relative accuracy' of the multipole expansion is of the order of 10^{-9} to 10^{-10}. For larger gaps, the uncertainty rapidly decreases with the distance and for $\ell/a - 1 \geqslant 0{\cdot}001$ the required 16 digits precision is easily obtained and exceeded by our 32-digit FORTRAN calculation. For a single sphere in modulated shear flow, the 32-digit ME accuracy is obtained for the whole range of distances, even at the contact. All the calculated values are in perfect agreement with the ones obtained by Pasol *et al.* from the bipolar coordinates method in the companion paper (**20**).

For practical applications, to reach the one per cent relative accuracy of the forces and torques on a motionless sphere, the multipole order $L = 3$ is sufficient. A motion of the sphere with respect to a very close wall requires significantly more multipoles, or a more elaborate treatment: subtracting the lubrication expressions from the friction coefficients, and calculating the rest as a fast-convergent series in inverse powers of the distance from the sphere centre to the wall, ℓ/a. With no ambient flow, the one per cent absolute precision is obtained already for truncation at as low power as $n = 8$. Actually, the power series with $n = 450$ can also be used with no substantially larger computational cost. Then, for small gaps $\ell/a - 1 \leqslant 10^{-2}$, the precision is not worse than 10^{-7}; for larger gaps at least 16 digits are precise. For all the distances, the absolute precision is evaluated (and improved) from (5.3), using coefficients of lubrication asymptotic expressions. Note how strong is this result, taking into account that the lubrication expressions are applicable for very close distances only. Our analysis indicates that precise calculation of Chaoui and Feuillebois (**24**) of the lubrication coefficients in bipolar coordinates may be used to significantly improve accuracy of the power series. Such a series is used in many-body systems to construct pairwise lubrication corrections, which account for interactions between each sphere and the wall, and also between two spheres. Such lubrication corrections, after (**33**), are used in the Stokesian dynamics (**4**, **19**) and in the statistical description of suspensions, in a similar way as in (**34**). The multipole method used in this paper can currently treat up to around one hundred spheres, plus one or two plane walls.

Acknowledgement

We thank Professor François Feuillebois for helpful discussions and useful remarks on the manuscript. We are grateful to Professor François Feuillebois, Dr Laurentiu Pasol and Professor Antoine

Sellier for sharing results of their calculation in bipolar coordinates with us. Visits of the first author to France were supported by a PAN-CNRS grant.

References

1. J. K. G. Dhont, *An Introduction to Dynamics of Colloids* (Elsevier, Amsterdam 1996).
2. S. Kim and S. J. Karrila, *Microhydrodynamics. Principles and Selected Applications* (Dover, Mineola 2005).
3. A. Satoh, *Introduction to Molecular-Microsimulation of Colloidal Dispersions* (Elsevier, Amsterdam 2003).
4. J. F. Brady and G. Bossis, Stokesian dynamics, *Ann. Rev. Fluid Mech.* **20** (1988) 111–157.
5. A. J. C. Ladd, Hydrodynamic transport coefficients of random dispersions of hard spheres, *J. Chem. Phys.* **95** (1990) 3484–3494.
6. A. Sierou and J. F. Brady, Accelerated Stokesian dynamics simulations, *J. Fluid Mech.* **448** (2001) 115–146.
7. B. Cichocki, R. B. Jones, R. Kutteh and E. Wajnryb, Friction and mobility for colloidal spheres in Stokes flow near a boundary: the multipole method and applications, *J. Chem. Phys.* **112** (2000) 2548–2561.
8. R. B. Jones, Spherical particle in Poiseuille flow between planar walls, *J. Chem. Phys.* **121** (2004) 483–500.
9. S. Bhattacharya, J. Bławzdziewicz and E. Wajnryb, Hydrodynamic interactions of spherical particles in suspensions confined between two planar walls, *J. Fluid Mech.* **541** (2005) 263–292.
10. I. L. Claeys and J. F. Brady, Lubrication singularities of the grand resistance tensor for two arbitrary particles, *PCH PhysicoChemical Hydrodynamics* **11** (1989) 261–293.
11. A. S. Sangani and G. Mo, Inclusion of lubrication forces in dynamic simulations, *Phys. Fluids* **6** (1994) 1653–1662.
12. N.-Q. Nguyen and A. J. C. Ladd, Lubrication corrections for lattice-Boltzmann simulations of particle suspensions, *Phys. Rev.* E **66** (2002) 046708-1–12.
13. O. A. Ladyzhenskaya, *The Mathematical Theory of Viscous Incompressible Flow* (Gordon & Breach, New York 1969).
14. C. Pozrikidis, *Boundary Integral and Singularity Methods for Linearized Viscous Flow* (Cambridge University Press, Cambridge 1992).
15. J. R. Blake, A note on the image system for a Stokeslet in a no-slip boundary, *Proc. Camb. Phil. Soc.* **70** (1971) 303–310.
16. B. Cichocki and R. B. Jones, Image representation of a spherical particle near a hard wall, *Physica* A **258** (1998) 273–302.
17. H. A. Lorentz, A general theorem concerning the motion of a viscous fluid and a few consequences derived from it, *Versl. K. Akad. W. Amsterdam* **5** (1897) 168.
18. R. Schmitz and B. U. Felderhof, Creeping flow about a spherical particle, *Physica* A **113** (1982) 90–102.
19. B. Cichocki, B. U. Felderhof, K. Hinsen, E. Wajnryb and J. Bławzdziewicz, Friction and mobility of many spheres in Stokes flow, *J. Chem. Phys.* **100** (1994) 3780–3790.
20. L. Pasol, A. Sellier and F. Feuillebois, A sphere in a second degree polynomial creeping flow parallel to a wall, *Q. Jl Mech. Appl. Math.* **59** (2006) 587–614.

21. R. G. Cox and H. Brenner, Effect of finite boundaries on the Stokes resistance of an arbitrary particle: Part 3. Translation and rotation, *J. Fluid Mech.* **28** (1967) 391–411.
22. P. Mazur and D. Bedeaux, A generalization of Faxén's theorem to nonsteady motion of a sphere through an incompressible fluid in arbitrary flow, *Physica* **76** (1974) 235–246.
23. B. U. Felderhof, Force density induced on a sphere in linear hydrodynamics, *Physica* A **84** (1976) 557–576.
24. M. Chaoui and F. Feuillebois, Creeping flow around a sphere in shear flow close to a wall, *Q. Jl Mech. Appl. Math.* **56** (2003) 381–410.
25. J. M. Normand, *A Lie Group: Rotations in Quantum Mechanics* (North–Holland, Amsterdam 1980).
26. A. R. Edmonds, *Angular Momentum in Quantum Mechanics* (Princeton University Press, Princeton 1974).
27. R. Schmitz and B. U. Felderhof, Friction matrix for two spherical particles with hydrodynamic interaction, *Physica* A **113** (1982) 103–116.
28. S. L. Goren and M. E. O'Neill, On the hydrodynamic resistance to a particle of a dilute suspension when in the neighborhood of a large obstacle, *Chem. Engng Sci.* **26** (1971) 325–338.
29. D. J. Jeffrey and Y. Onishi, Calculation of the resistance and mobility functions for two unequal rigid spheres in low-Reynolds-number flow, *J. Fluid Mech.* **139** (1984) 261–290.
30. A. J. Goldman, R. G. Cox and H. Brenner, Slow viscous motion of a sphere parallel to a plane wall. I. Motion through a quiescent flow, *Chem. Engng Sci.* **22** (1967) 637–651.
31. M. E. O'Neill and K. Stewartson, On the slow motion of a sphere parallel to a nearby wall, *J. Fluid Mech.* **27** (1967) 705–724.
32. A. J. Goldman, R. G. Cox and H. Brenner, Slow viscous motion of a sphere parallel to a plane wall. I. Couette flow. *Chem. Engng Sci.* **22** (1967) 653–660.
33. L. Durlofsky, J. F. Brady and G. Bossis, Dynamic simulation of hydrodynamically interacting particles, *J. Fluid Mech.* **180** (1987) 21–49.
34. B. Cichocki, M. L. Ekiel-Jeżewska and E. Wajnryb, Lubrication corrections for three-particle contribution to short-time self-diffusion coefficients in colloidal dispersions, *J. Chem. Phys.* **111** (1999) 3265–3273.

APPENDIX A

How do force- and velocity-multipoles relate to physical quantities?

The force $\boldsymbol{F}$ and the torque $\boldsymbol{C}$, exerted by the fluid on the sphere, are expressed in terms of the force multipoles as

$$\boldsymbol{F} = \begin{pmatrix} F_x \\ F_y \\ F_z \end{pmatrix} = \sqrt{\frac{4\pi}{3}} \begin{pmatrix} f(1\,1\,0) \\ f(1\text{–}1\,0) \\ -f(1\,0\,0) \end{pmatrix}, \quad \boldsymbol{C} = \begin{pmatrix} C_x \\ C_y \\ C_z \end{pmatrix} = \sqrt{\frac{4\pi}{3}} \begin{pmatrix} f(1\,1\,1) \\ f(1\text{–}1\,1) \\ -f(1\,0\,1) \end{pmatrix}. \tag{A.1}$$

The translational and angular velocities of the sphere are expressed by the velocity multipoles as

$$\boldsymbol{U} = \begin{pmatrix} U_x \\ U_y \\ U_z \end{pmatrix} = \sqrt{\frac{3}{4\pi}} \begin{pmatrix} -c_0(1\,1\,0) \\ -c_0(1\text{–}1\,0) \\ c_0(1\,0\,0) \end{pmatrix}, \quad \boldsymbol{\Omega} = \begin{pmatrix} \Omega_x \\ \Omega_y \\ \Omega_z \end{pmatrix} = \sqrt{\frac{3}{4\pi}} \begin{pmatrix} -c_0(1\,1\,1) \\ -c_0(1\text{–}1\,1) \\ c_0(1\,0\,1) \end{pmatrix}. \tag{A.2}$$

At the centre of the sphere, the ambient flow and its derivatives of all orders are expressed by the corresponding velocity multipoles c_∞. In particular,

$$\boldsymbol{u}_\infty(\boldsymbol{\ell}) = \sqrt{\frac{3}{4\pi}} \begin{pmatrix} -c_\infty(1\,1\,0) \\ -c_\infty(1{-}1\,0) \\ c_\infty(1\,0\,0) \end{pmatrix}, \quad \frac{1}{2}\nabla \times \boldsymbol{u}_\infty(\boldsymbol{\ell}) = \sqrt{\frac{3}{4\pi}} \begin{pmatrix} -c_\infty(1\,1\,1) \\ -c_\infty(1{-}1\,1) \\ c_\infty(1\,0\,1) \end{pmatrix}. \tag{A.3}$$

APPENDIX B

Ambient flows as combinations of the multipole vector functions

According to (3.5), the ambient fluid flows $\boldsymbol{u}_\infty(\boldsymbol{x})$ at any point $\boldsymbol{x}$ in the fluid may be expressed as superposition of multipole vector functions, $\boldsymbol{u}^+_{lm\sigma}(\boldsymbol{X})$, with the position $\boldsymbol{X} = \boldsymbol{x} - \boldsymbol{\ell}$ measured with respect to the sphere centre $\boldsymbol{\ell} = [0, 0, \ell]$; see Fig. 1. The basic set of these functions was defined in (**7**). We explicitly write below the decomposition (3.5) for the pure shear, quadratic, and modulated shear flows. In all these cases, the sums in (3.5) consist of only several terms. It is convenient to denote

$$\tilde{\mathbf{u}}^+_{lm\sigma} = \frac{\mathbf{u}^+_{lm\sigma}}{\Gamma_l}, \quad \text{with } \Gamma_l = \sqrt{\frac{l(2l+1)!!}{4\pi(l-1)!}}. \tag{B.1}$$

Using this notation, with $\boldsymbol{x} = (x, y, z)$ and $\boldsymbol{X} = (X, Y, Z) = (x, y, z - \ell)$, as defined in Fig. 1, we write the pure shear, quadratic, and modulated shear flows as

$$z\,\mathbf{e}_x = -\ell\tilde{\mathbf{u}}^+_{110}(\boldsymbol{X}) - \frac{1}{2}\tilde{\mathbf{u}}^+_{1-11}(\boldsymbol{X}) - \frac{1}{\sqrt{2}}\tilde{\mathbf{u}}^+_{210}(\boldsymbol{X}), \tag{B.2}$$

$$\begin{aligned} z^2\,\mathbf{e}_x = &-\ell^2\tilde{\mathbf{u}}^+_{110}(\boldsymbol{X}) - \ell\tilde{\mathbf{u}}^+_{1-11}(\boldsymbol{X}) - \sqrt{2}\ell\tilde{\mathbf{u}}^+_{210}(\boldsymbol{X}) \\ &- \frac{1}{15}\tilde{\mathbf{u}}^+_{112}(\boldsymbol{X}) - \frac{\sqrt{2}}{3}\tilde{\mathbf{u}}^+_{2-11}(\boldsymbol{X}) - \frac{2}{\sqrt{15}}\tilde{\mathbf{u}}^+_{310}(\boldsymbol{X}), \end{aligned} \tag{B.3}$$

$$\begin{aligned} 2yz\,\mathbf{e}_x = &\sqrt{2}\ell\tilde{\mathbf{u}}^+_{2-20}(\boldsymbol{X}) - \frac{\sqrt{2}}{3}\tilde{\mathbf{u}}^+_{221}(\boldsymbol{X}) + \sqrt{\frac{2}{3}}\tilde{\mathbf{u}}^+_{3-20}(\boldsymbol{X}) \\ &- \ell\tilde{\mathbf{u}}^+_{101}(\boldsymbol{X}) - \sqrt{\frac{2}{3}}\tilde{\mathbf{u}}^+_{201}(\boldsymbol{X}). \end{aligned} \tag{B.4}$$

The multipole vector functions $\tilde{\mathbf{u}}^+_{lm\sigma}$ appearing in (B.4) have the form

$$\tilde{\mathbf{u}}^+_{110}(\boldsymbol{X}) = [-1, 0, 0], \tag{B.5}$$

$$\tilde{\mathbf{u}}^+_{1-11}(\boldsymbol{X}) = [-Z, 0, X], \tag{B.6}$$

$$\tilde{\mathbf{u}}^+_{210}(\boldsymbol{X}) = \frac{1}{\sqrt{2}}[-Z, 0, -X], \tag{B.7}$$

$$\tilde{\mathbf{u}}^{+}_{112}(\boldsymbol{X}) = [-3(X^2 + 2Y^2 + 2Z^2), 3XY, 3XZ], \tag{B.8}$$

$$\tilde{\mathbf{u}}^{+}_{2-11}(\boldsymbol{X}) = \frac{1}{\sqrt{2}}[Y^2 - Z^2, -XY, -XZ], \tag{B.9}$$

$$\tilde{\mathbf{u}}^{+}_{310}(\boldsymbol{X}) = \frac{1}{2\sqrt{15}}[3X^2 + Y^2 - 4Z^2, 2XY, -8XZ], \tag{B.10}$$

$$\tilde{\mathbf{u}}^{+}_{101}(\boldsymbol{X}) = [-Y, X, 0], \tag{B.11}$$

$$\tilde{\mathbf{u}}^{+}_{2-20}(\boldsymbol{X}) = \frac{1}{\sqrt{2}}[Y, X, 0], \tag{B.12}$$

$$\tilde{\mathbf{u}}^{+}_{201}(\boldsymbol{X}) = \sqrt{\frac{3}{2}}[-YZ, XZ, 0], \tag{B.13}$$

$$\tilde{\mathbf{u}}^{+}_{221}(\boldsymbol{X}) = \frac{1}{\sqrt{2}}[-YZ, -XZ, 2XY], \tag{B.14}$$

$$\tilde{\mathbf{u}}^{+}_{3-20}(\boldsymbol{X}) = \sqrt{\frac{2}{3}}[YZ, XZ, XY]. \tag{B.15}$$

APPENDIX C

Evaluation of friction factors

The force multipoles are now calculated. The forces and torques on a moving sphere are calculated from equation (3.7), with c_0 related to the translational and angular velocities as in Appendix A. For the forces and torques exerted on the sphere in the ambient fluid flow, equation (3.8) is applied, with the coefficients c_∞, determined in Appendix B. The resulting friction factors are

$$f^{\mathrm{t}}_{xx}(L) = \frac{2}{9\mu a} Z_L(110, 110), \tag{C.1}$$

$$c^{\mathrm{t}}_{yx}(L) = -\frac{1}{6a^2\mu} Z_L(1\,{-}11, 110), \tag{C.2}$$

$$f^{\mathrm{r}}_{xy}(L) = -\frac{2}{9a^2\mu} Z_L(110, 1\,{-}11), \tag{C.3}$$

$$c^{\mathrm{r}}_{yy}(L) = \frac{1}{6a^3\mu} Z_L(1\,{-}11, 111), \tag{C.4}$$

$$c^{\mathrm{r}}_{zz}(L) = \frac{1}{6a^3\mu} Z_L(101, 101), \tag{C.5}$$

$$f^{\mathrm{s}}_{xx}(L) = \frac{1}{9a\ell\mu}\left[2\ell Z_L(110,110) + Z_L(110,1\,{-}11) + \frac{1}{\sqrt{5}}Z_L(110,210)\right], \tag{C.6}$$

$$c^{\mathrm{s}}_{yx}(L) = \frac{1}{6a^3\mu}\left[2\ell Z_L(1\,{-}11,110) + Z_L(1\,{-}11,1\,{-}11) + \frac{1}{\sqrt{5}}Z_L(1\,{-}11,210)\right], \tag{C.7}$$

$$f^{\mathrm{q}}_{xx}(L) = \frac{2}{9a\ell^2\mu}\left[\ell^2 Z_L(110,110) + \ell Z_L(110,1\,{-}11) + \frac{\ell}{\sqrt{5}}Z_L(110,210) + \frac{1}{15}Z_L(110,112) + \frac{1}{3\sqrt{5}}Z_L(110,2\,{-}11) + \frac{2\sqrt{2}}{15\sqrt{7}}Z_L(110,310)\right], \tag{C.8}$$

$$c^{\mathrm{q}}_{yx}(L) = \frac{1}{6a^3\ell\mu}\left[\ell^2 Z_L(1\,{-}11,110) + \ell Z_L(1\,{-}11,1\,{-}11) + \frac{\ell}{\sqrt{5}}Z_L(1\,{-}11,210) + \frac{1}{15}Z_L(1\,{-}11,112) + \frac{1}{3\sqrt{5}}Z_L(1\,{-}11,2\,{-}11) + \frac{2\sqrt{2}}{15\sqrt{7}}Z_L(1\,{-}11,310)\right], \tag{C.9}$$

$$c^{\mathrm{m}}_{zx}(L) = \frac{1}{6a^3\ell\mu}\left[\ell Z_L(101,101) + \frac{1}{\sqrt{15}}Z_L(101,201)\right]. \tag{C.10}$$

Note that due to the Lorentz symmetry, $Z_L(lm\sigma,l'm'\sigma') = Z_L(l'm'\sigma',lm\sigma)$ and, due to the axial symmetry, $Z_L(lm\sigma,l'm'\sigma') = 0$ for $m \neq \pm m'$. Moreover, for large ℓ/a the leading non-constant terms of $Z_L(lm\sigma,l'm'\sigma')$ scale as $\sim(\ell/a)^{-(l+l'+\sigma+\sigma'-1)}$.

For $\xi = \ell/a - 1 \ll 1$, the friction factors f^{t}_{xx}, $c^{\mathrm{t}}{}_{yx}$ and c^{r}_{yy} diverge as $A\ln\xi$, with $A^{\mathrm{t}}_{xx} = -\frac{8}{15}$, $A^{\mathrm{t}}{}_{yx} = -\frac{1}{10}$, $A^{\mathrm{r}}_{yy} = -\frac{2}{5}$, see (**30**, **31**). Therefore

$$\lim_{\xi\to 0}\left(\frac{c^{\mathrm{t}}{}_{yx}}{f^{\mathrm{t}}{}_{xx}}\right) = \frac{A^{\mathrm{t}}_{yx}}{A^{\mathrm{t}}_{xx}} = \frac{3}{16} \qquad \text{and} \qquad \lim_{\xi\to 0}\left(\frac{c^{\mathrm{r}}_{yy}}{f^{\mathrm{t}}_{xx}}\right) = \frac{A^{\mathrm{r}}_{yy}}{A^{\mathrm{t}}_{xx}} = \frac{3}{4}. \tag{C.11}$$

Finally, it is interesting to discuss the dependence of the friction factors on the multipole order L. Both $f^{\mathrm{t}}_{xx}(L)$ and $c^{\mathrm{r}}_{yy}(L)$ are strictly increasing functions of L, because the friction matrix $\mathbf{Z}_L$ is symmetric and positive-definite for arbitrary ℓ/a. From this property it follows that c^{t}_{yx} is also an increasing function of L, if ℓ/a is sufficiently small, because in this case the leading contributions to the friction factors (proportional to $\ln\xi$) are related to each other by (C.11). Moreover, for very large ℓ/a, $f^{\mathrm{q}}_{xx}(L)$ and $f^{\mathrm{s}}_{xx}(L)$ are increasing functions of L, because according to (C.6) and (C.8), their leading contributions, proportional to a/ℓ, arise from f^{t}_{xx}.

APPENDIX D

Values of friction factors f^{t}_{xx}, c^{t}_{yx} and c^{r}_{yy}

Values of the friction factors f^{t}_{xx}, c^{t}_{yx}, and c^{r}_{yy} have been precisely calculated in bipolar coordinates in (**20**). Here we recalculate the same values by the multipole expansion, and list them in Table D1, as a reference for the calculated precision.

Table D1 Friction factors f^{t}_{xx}, c^{t}_{yx} and c^{r}_{yy} for a sphere centred at a distance ℓ from the wall, calculated by the inverse-power expansion (for $\ell/a \leqslant 1{\cdot}0001$) and by the pure multipole expansion (for $\ell/a \geqslant 1{\cdot}001$)

ℓ/a	f^{t}_{xx}	c^{t}_{yx}	c^{r}_{yy}
1·000002	7·95289287	1·11928831	5·6198525
1·000005	7·46421170	1·02766552	5·2533556
1·00001	7·09454458	0·95836061	4·9761270
1·0001	5·86667539	0·72824978	4·0555491
1·001	4·640038165209212	0·499111844773750	3·137983756794614
1·005	3·7867298869201254	0·3419456909933512	2·5059413761990461
1·01	3·4225329663656397	0·2765174026634165	2·2407976493684943
1·05	2·5989632789810749	0·1379253408245965	1·6674610087470452
1·1	2·2643030353880285	0·0887633441741130	1·4548512100169826
1·2	1·9527071178778222	0·0496376581486575	1·2766391754162502
1·5	1·5957066189809054	0·0165739619041205	1·1104954933381374
2·0	1·3827523824112231	0·0050247112290880	1·0417835548066169
4·0	1·1619560820699792	0·0003318077201772	1·0049215496715140
5·0	1·1258610645109942	0·0001385021924306	1·0025100848288520
10·0	1·0594825555256237	0·0000090119714614	1·0003126564736819
21·0	1·0275096534244965	0·0000004732608454	1·0000337454784515
51·0	1·0111514796398637	0·0000000137547589	1·0000023558147164